From magnetic order to spin-liquid ground states on the S=3/2 triangular lattice

J. Tapp, C. R. dela Cruz, M. Bratsch, N. E. Amuneke, L. Postulka, B. Wolf, M. Lang, H. O. Jeschke, R. Valentí, P. Lemmens, and A. Möller

Phys. Rev. B **96**, 064404 — Published 3 August 2017

DOI: 10.1103/PhysRevB.96.064404

From magnetic order to spin liquid ground states on the $S = 3/2$ triangular lattice

J. Tapp,[1] C. R. dela Cruz,[2] M. Bratsch,[3] N. E. Amuneke,[3] L. Postulka,[4] B. Wolf,[4] M. Lang,[4] H. O. Jeschke,[5] R. Valentí,[5] P. Lemmens,[6] and A. Möller*[1]

[1]*Institute for Inorganic Chemistry and Analytical Chemistry, JGU Mainz, Duesbergweg 10-14, 55128 Mainz, Germany*

[2]*Quantum Condensed Matter Division, Oak Ridge National Laboratory, Oak Ridge Tennesee 37831, USA*

[3]*Department of Chemistry, University of Houston, Texas 77204-5003, USA*

[4]*Physikalisches Institut, Goethe-Universität Frankfurt, Max-von-Laue-Straße 1, 60438 Frankfurt am Main, Germany*

[5]*Institut für Theoretische Physik, Goethe-Universität Frankfurt, Max-von-Laue-Straße 1, 60438 Frankfurt am Main, Germany*

[6]*Institute for Physics of Condensed Matter, TU Braunschweig, Mendelsohnstr. 3, 38106 Braunschweig, Germany*

(Dated: July 17, 2017)

Abstract

The series of compounds, $AAg_2Cr[VO_4]_2$ with A = Ag, K, or Rb, are layered $S = 3/2$ triangular-lattice (TL) systems where the magnetic exchange interactions between Cr^{3+} ($3d^3$) ions are mediated by non-magnetic $[VO_4]^{3-}$ entities. Here, the relative orientation of the vanadate is altered with respect to the TL as a function of the A-site which corresponds to an induced symmetry change of the $[CrO_6]$-complex. All members of this series of compounds belong to the class of frustrated TL antiferromagnets. We find that the distorted TL (A = Ag) exhibits collinear antiferromagnetic long-range order (LRO) at $T_N \approx 10\,\mathrm{K}$, whereas the high-symmetry cases (A = K, Rb) evade LRO in zero field down to 0.03 K, the lowest temperature of our experiments. The latter members of the series belong to the undistorted TL and are candidates for spin-liquid ground states presumably not related to Ising anisotropy or dimerization.

I. INTRODUCTION

In recent years, considerable effort has been devoted to the fascinating properties of spin liquids (SL)[1–4] and their relevance for possible applications such as quantum computation[5]. Some of the most successful approaches towards a rational design of such materials rely on the geometrical frustration of the Heisenberg spin exchange on triangular, kagome and pyrochore lattices[2,6–9] or, more recently, on the presence of spin-orbit induced anisotropic interactions on the honeycomb lattice[10,11]. One important ingredient to novel frustrated materials is the adherence to strict geometrical guidelines, i.e. three-fold rotation symmetry for the triangular lattice (TL), which remains a considerable challenge in synthesis. The importance of the symmetry aspect has been pointed out by theory as it effectively suppresses additional terms of the Hamiltonian which may otherwise induce long-range order (LRO)[3,12–14].

The Heisenberg model on the undistorted TL (equilateral triangles of three-fold symmetry) with a nearest-neighbor exchange parameter (J) is a conceptually important model[3,5]. Irrespective of the spin magnitude, LRO is predicted by theory for the antiferromagnetic (AFM) Heisenberg model on the TL with an exceptional ground state that corresponds to a chiral 120° arrangement of magnetic moments[5,14–16]. However, LRO may be suppressed for large single-ion anisotropies on the undistorted Ising AFM-TL in favor of a spin-liquid like ground state with large remaining entropy[17]. Quasi two-dimensional materials that present a good realization of the undistorted TL are rare. Examples for Heisenberg systems with very weak single-ion anisotropies are $ACrO_2$[18], $RbFe[MoO_4]_2$[19] and $AAg_2Fe[VO_4]_2$[20]. The latter Fe-compounds belong to the class of XY-Heisenberg TL and order antiferromagnetically around 3 K. For $ACrO_2$ a very small uniaxial anisotropy has been reported and the ground state represents the solution for the easy-axis Heisenberg model on the TL[21]. Even for the most prominent Ising-ion candidate of the $3d$-ion series, Co^{2+}, chiral 120° LRO has been established, see for example $Ba_3CoSb_2O_9$[13].

Beyond the single-ion anisotropy other approaches have been considered to effectively destabilize LRO on the TL. These include (i) spatial anisotropy leading to different nearest-neighbor coupling constants (J_1, J_2), or (ii) further couplings beyond nearest-neighbor two-spin exchange. It has been theoretically shown for $S = 1/2$ systems that SL ground states can be realized for very large differences or certain ratios of J_1 and J_2[22,23]. As spatial anisotropies are not expected for the undistorted TL, scenario (ii) with multiple spin exchange could

apply[24,25]. Such consecutive exchange processes can effectively suppress AFM LRO as these induce a ferromagnetic component[26,27]. The unambiguous detection is far from trivial as it modifies the physical properties only gradually. Nevertheless, higher order exchange has been proposed for systems were effective Coulomb correlations are weaker and/or the exchange path involves several ions[28].

In the present study we focus on members of the $AAg_2M[VO_4]_2$ series of compounds which exhibit tunable ion sites: A and M[20,29,30]. For the magnetic ion (M-site) we have chosen the Heisenberg ion Cr^{3+} ($3d^3$) here, because of its extremely small single-ion anisotropy and its orbitally non-degenerate ground state, ${}^4A_{2g}$, in an octahedral ligand field. The tuning of the magnetic exchange interactions through (M3d−O2p−V3d−O2p−M3d) hybridization is accomplished by the size of the non-magnetic ion on the A-site. Thereby, rotation and/or tilting of the linker $[VO_4]^{3-}$ occurs, see Figure 1. Here, we present experimental data on a novel insulating Cr-series, reporting the suppression of LRO and evidence for a SL-like state due to high-symmetry exchange on the $S = 3/2$ AFM TL.

II. EXPERIMENTAL DETAILS

The samples have been obtained from initial reaction of K_2CO_3 (Rb_2CO_3, or Ag_2O) with Cr_2O_3 and $AgVO_4$ in molar ratios of $1:1:4$ at 753 K, followed by consecutive annealings of pressed pellets at approximately 773 K. The sample quality has been checked by powder x-ray diffraction (Cu-K_α radiation, Bruker D 5000 or XPert Pro PANanalytical instruments). The neutron diffraction measurements were done using the HB2a high resolution powder diffractometer housed at the High Flux Isotope reactor, Oak Ridge National Laboratory. The pelletized powder samples were measured as a function of temperature using a ^{3}He-insert. The collimation used for the measurement was open-open-12′, before the monochromator, sample and detector, respectively, with the Ge[113] wavelength of 2.406 Å. X-ray and neutron data were refined using the program $FullProf$[31].

DC-Susceptibility measurements of pressed powder samples were carried out on a physical properties measurement system (PPMS, Quantum Design) using the vibrating sample magnetometer (VSM) option and a commercial SQUID magnetometer (MPMS). The measurements were performed in the range of $2\,\mathrm{K} \leq T \leq 300\,\mathrm{K}$ in zero field cooled (zfc) and field cooled (fc) mode at a field of 0.1 T (see below) and up to 1 T. Field dependent magnetiza-

tion data were collected at 2 K in fields up to 8 T. The experimental data were corrected for the contribution of the sample holder which was determined in an independent experiment and for temperature-independent diamagnetic core contributions[32]. For measurements of the ac-susceptibility, χ_{ac}, down to $T = 0.031$ K and magnetic fields up to 10 T, an ultra-high resolution ac-susceptometer, adapted to a ^{3}He-^{4}He top-loading dilution refrigerator was used. Specific heat measurements were performed using a PPMS instrument within a temperature range of 2-300 K in magnetic fields of 0-8 T. Phonon contributions were subtracted from the specific heat data by using the non-magnetic structural analogues with M = In and A = Ag, K, Rb, respectively.

III. RESULTS AND DISCUSSION

A. Crystallographic and Magnetic Structure

We refined the crystal structures of $AAg_2Cr[VO_4]_2$ with A = Ag, K, and Rb from powder neutron (NPD) and x-ray diffraction data. For further details, we refer to the supplement[33]. The compounds crystallize in the space group $P\bar{3}$ for A = K, Rb and $C2/c$ for A = Ag (Figure 1). The prominent feature of these structures is a TL of magnetic Cr^{3+} ions (S = 3/2) linked by non-magnetic vanadate units, $[VO_4]^{3-}$, as shown in Figure 1 (c,d). The two structure types differ in the local symmetry of the $[CrO_6]$-units: D_{3d} symmetry with O−Cr−O angles of 90° (Rb) and 89° / 91° (K) for $P\bar{3}$ (undistorted TL) versus C_{2v} symmetry with O−Cr−O of 85.9°, 88.1°, 91.2° (Ag) for $C2/c$ (undistorted TL). In the former case the connecting vanadate units are coplanar with the TL, whereas in the latter case these are tilted with respect to the axis perpendicular to the TL. Thus, the two structures differ in terms of the ideal equilateral TL ($P\bar{3}$, A = K, Rb) with Cr-Cr distances of 5.443 Å and a distorted TL ($C2/c$, A = Ag) with 5.094 Å and 2 × 5.482 Å. The inter-layer distance along the stacking direction (c-axis) is 7.173 Å (Ag), 7.236 Å (K), and 7.345 Å (Rb), respectively, and follows approximately the increasing ionic size of the A-site cations.

In Figure 2 (a,b), we show the measured neutron diffraction data at 5 K, 2 K, and 260 mK for the undistorted TL ($P\bar{3}$, $RbAg_2Cr[VO_4]_2$). The crystal structure contains two independent O-atoms. One is linking the Cr- and V-atoms within the TL whereas the other O-atom connects exclusively the non-magnetic cations. Therefore, the magnetic exchange can be as-

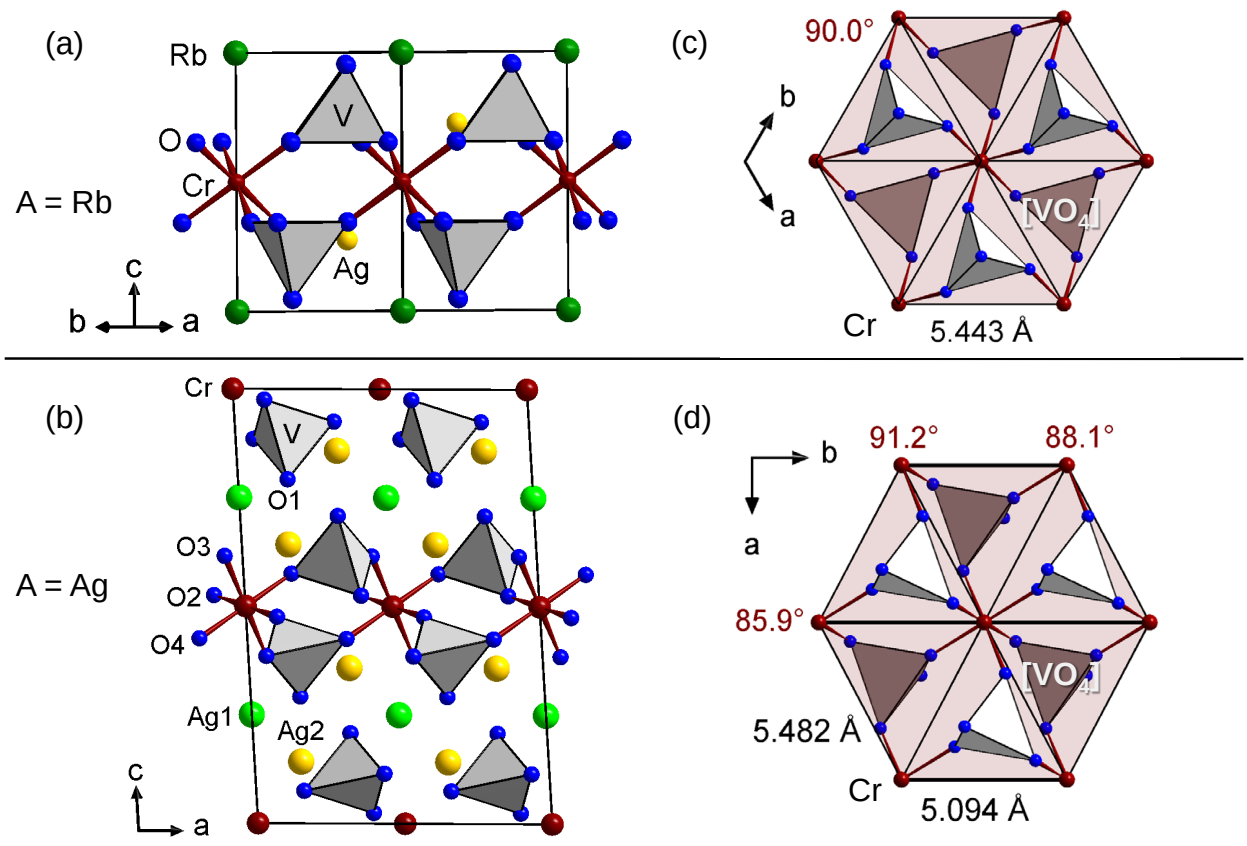

FIG. 1. (*Color online*) (*Left*): Crystal structures of (a) $RbAg_2Cr[VO_4]_2$ ($P\bar{3}$) and (b) $AgAg_2Cr[VO_4]_2$ ($C2/c$). (*Right*): Cr atoms linked via $[VO_4]$ entities on the TL: (c) undistorted case for A = Rb and (d) distorted case A = Ag. The Cr-Cr distances (black) and O-Cr-O angles (red) are given for comparison.

signed to a single J-parameter for the nearest neighbors. The retained threefold symmetry down to the lowest measured temperatures makes this compound an exceptional candidate for geometrical frustration scenarios. Thus, one expects significant suppression of LRO in comparison to a distorted TL, see below A = Ag. For A = Rb we observe in the neutron diffraction experiments down to 260 mK only structural reflections (Bragg positions (001), (100), and (101) below $Q = 1.7\,\text{Å}^{-1}$), Figure 2 (b). Neither magnetic short-range order nor LRO down to 260 mK is detected within the experimental resolution, see difference plot.

In contrast, the distorted TL orders antiferromagnetically around $T_N \approx 10\,\text{K}$. Figure 2 (d) shows unambiguously additional magnetic reflections at 2 K in comparison with the structural reflections observed at 20 K. The propagation vector of the magnetic structure

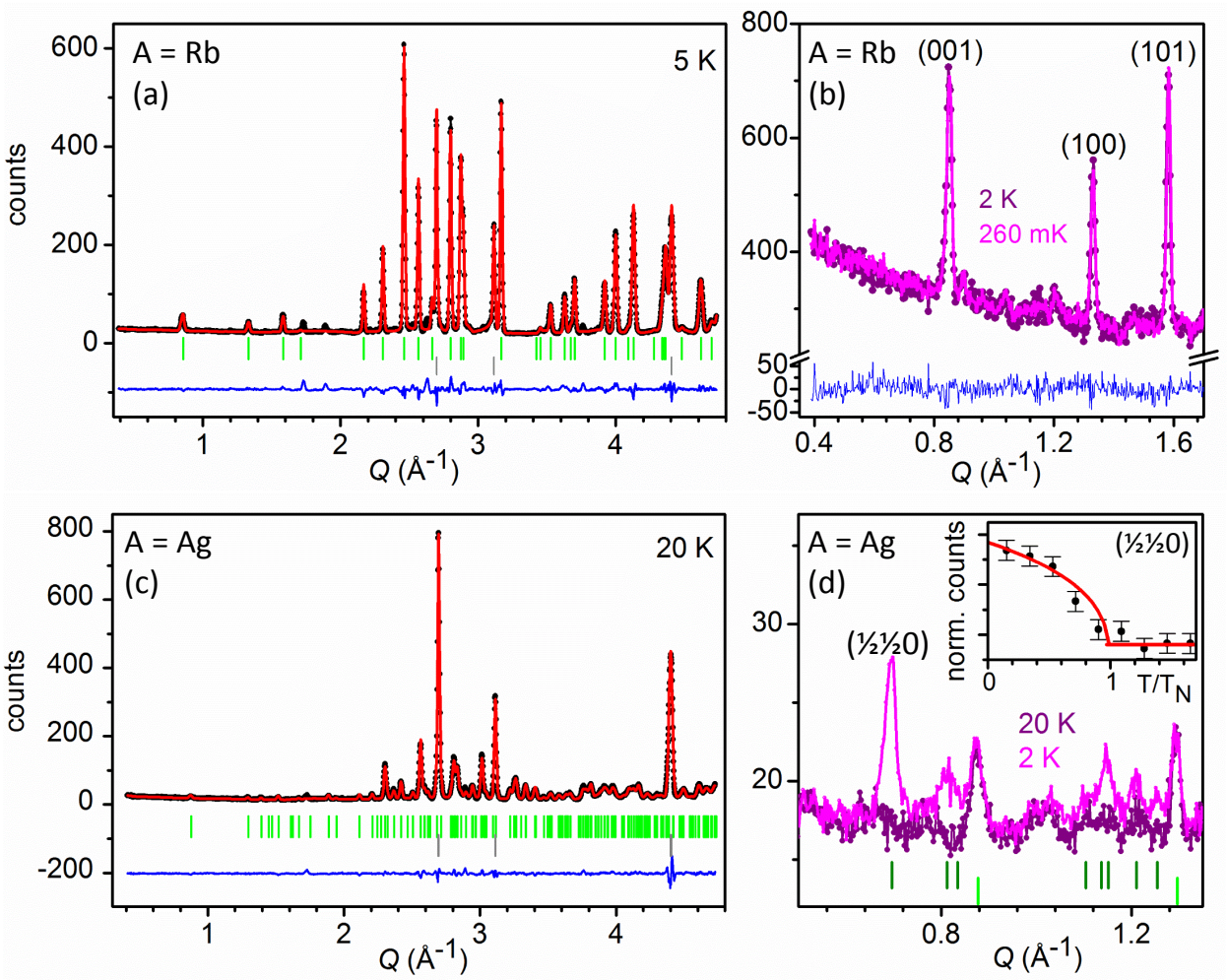

FIG. 2. (*Color online*) Rietveld refinement of the crystal structures of (a) $RbAg_2Cr[VO_4]_2$ ($P\bar{3}$) and (c) $AgAg_2Cr[VO_4]_2$ ($C2/c$); *black*: NPD data, *red*: simulated pattern, *green*: structural Bragg positions, *grey*: Bragg positions for aluminum (container), *blue*: difference observed-calculated. (b) Comparison of NPD for A = Rb at 260 mK and 2 K, difference (*blue*). (d) Comparison of NPD data for A = Ag at 2 K and 20 K, structural (*green*) and magnetic (*olive*) Bragg positions. The inset shows a fit of the order parameter for the magnetic reflection $(\frac{1}{2}\frac{1}{2}0)$, see text.

for $AgAg_2Cr[VO_4]_2$ has been derived as $k = (\frac{1}{2}, \frac{1}{2}, 0)$. The reduced magnetic moment per Cr^{3+} amounts to 2.06 μ_B ($z = \frac{1}{2}$) and 2.35 μ_B ($z = 0$), respectively. We have fitted the order parameter, β, of the collinear AFM phase by using the expression $y = |T/T_N - 1|^{\beta}$, where T_N equals the Néel temperature and y the normalized counts per 200 seconds for the magnetic reflection $(\frac{1}{2}\frac{1}{2}0)$ at $Q = 0.6967$ Å^{-1}, see inset Figure 2 (d). The derived parameter, $\beta = 0.33(1)$, for this fit is close to the Heisenberg solution for the TL, $\beta = 0.35$. It differs

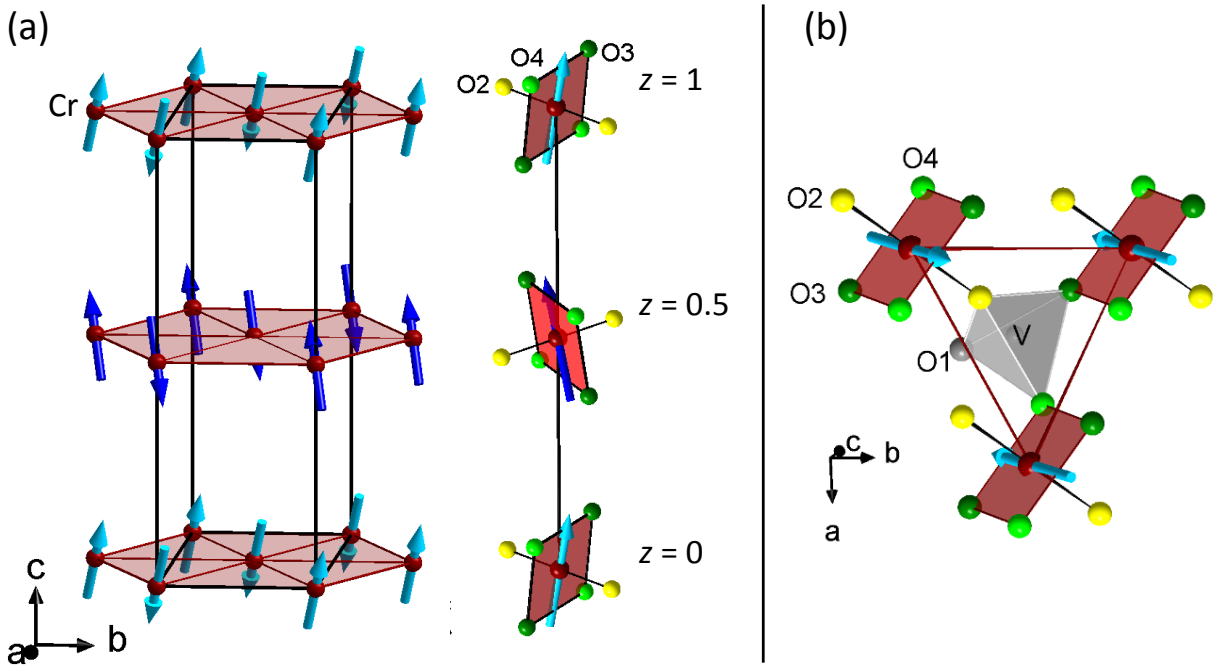

FIG. 3. (*Color online*) (a) Magnetic spin structure of the collinear AFM for A = Ag. The ordered magnetic moment is given with respect to the relative orientation of the [CrO_6]-complex along [001] and for one unit of the TL in (b).

from the Ising value of 1/8 and the mean field value of 0.5, respectively[15].

In Figure 3 we show the spin structure with the spins canted out of the TL plane. Note the AFM alignment of the spins along the shortest Cr-Cr distance, which is equivalent with the *b*-lattice constant. The two directions [110] and [-110] turn out to be aligned differently, despite the same Cr-Cr distances. Inspection of the O-Cr-O angles reveal the difference between the two crystallographic directions: 91.2° and 88.7° in [110] and [-110], respectively, see also Figure 1 (d). Thus, the relative orientation of the vanadate can be considered as the crucial ingredient to account for the non-equivalent magnetic exchange interactions. In the Ag-compound (distorted TL) four crystallographic distinguishable O-atoms exist. Out of these, three (O2, O3, O4) are exclusively connected to chromium. The ordered magnetic moment lies in the plane defined by Cr, O3, and O4 (Fig. 3). In the case that the magnetic exchange is mediated exclusively via O3 and O4 (represented by the [-110] direction), a FM alignment of the ordered magnetic moments is observed. In contrast, the other two Cr-Cr connectivities along [010] and [110] are bridged by the combination O2-O3 or O2-O4, respectively. For this case, the moments are found to align AFM. The alternating change in

orientation of Cr-O3-O4 plaquette along the $c-$axis is a result of the space group symmetry ($C2/c$). Accordingly, the ordered magnetic moments are canted with respect to the stacking direction. Furthermore, a FM alignment of these ordered moments along [001] is established and also supported by $ab-inito$ calculations below.

B. Magnetic Properties

We proceed now with the magnetic properties of the series of compounds $AAg_2Cr[VO_4]_2$ as shown in Figure 4. In all cases an effective magnetic moment of $\mu_{eff} = 3.8\,\mu_B$ at room temperature is observed which is consistent with the expectation for a $S = 3/2$ paramagnet. For all systems, the experimental susceptibility down to 2 K (Figure 4 (a)) is systematically smaller than the one calculated on the basis of a ligand field approach[34] for a single-ion complex of D_{3d} symmetry in zero field. Thus, the dominant exchange is AFM throughout the series. We derive Curie-Weiss temperatures of $\Theta_{CW}^{Ag} \approx$ -32 K, $\Theta_{CW}^{K} \approx$ -20 K, and $\Theta_{CW}^{Rb} \approx$ -10 K from fits in the high-temperature range. To determine the magnetic coupling constants, we fitted our data to a high-temperature series expansion (HTSE)[35] based on a $S = 3/2$ TL with Heisenberg interaction and g-factors (1.96) derived independently from EPR measurements: $J^{Ag} \approx 3$ K, $J^{K} \approx 1$ K, and $J^{Rb} \approx 0.5$ K, respectively.

These J-values for the K- and Rb-system determined using the HTSE agree very well with the ones obtained from the corresponding saturation fields $B_s(0)$ (see supplementary material). With the relation $B_s(0) = 9SJ$ we derive $J^{K} = 1.5$ K and $J^{Rb} = 0.6$ K. Note the small values of the exchange coupling constants due to the Cr-Cr interaction path via the $[VO_4]$ entities. The relative differences in J are significant considering that the average in-plane Cr-Cr distances of the series are almost identical (see above). More pronounced is the relative orientation of the vanadate which renders the J-value, i.e. with a ratio of six for J^{Ag}/J^{Rb}. It is also quite remarkable that a significant difference in $\chi(T)$ is observed for the K- and Rb-compound ($P\overline{3}$). One may relate the enhancement in χ or suppression in terms of J as an effective addition of a ferromagnetic component, which seems to be more pronounced once the $[CrO_6]$ entity is close to ideal O_h symmetry (A = Rb).

In the case of A = Ag a broad maximum in χ(T) around 20 K followed by a kink-like anomaly at $T_N \approx 10$ K indicates LRO well in line with the neutron and specific heat data (see below). The AFM exchange on a TL results in competing magnetic interactions which

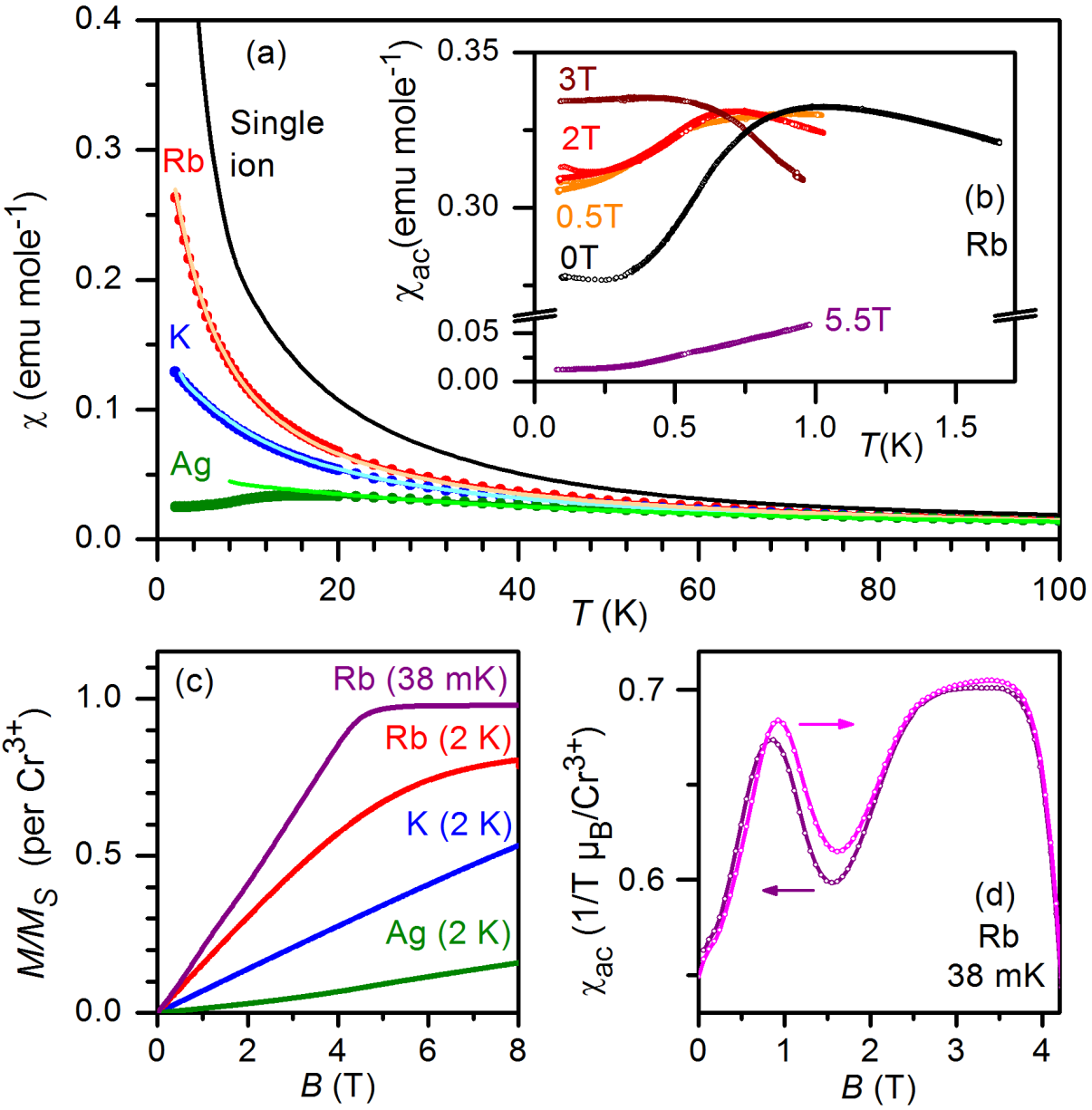

FIG. 4. (*Color online*) (a) Susceptibility data below 100 K for $AAg_2Cr[VO_4]_2$ with A = Ag (*green*), K (*blue*), Rb (*red*) measured in 0.1 T zfc mode in comparison with the calculated single ion data and fits to a HTSE for the TL (respective lines to the data). (b) *Inset.* χ_{ac}(T) for A = Rb below 1.7 K at various applied fields. (c) Magnetic moment divided by the saturated moment per Cr^{3+} vs. the applied field for A = Ag, K, Rb. (d) Hysteretic behavior of χ_{ac}(B) with increasing and decreasing fields (indicated by arrows) for A = Rb at 38 mK.

may be expressed by the ratio $\mid \Theta_{C.W.}/T_N \mid = f$[9]. For the distorted TL we find $\mid \Theta^{Ag}_{C.W.}/T^{Ag}_N \mid \approx 3$, which corresponds to a moderate frustration.

The inset (b) of Figure 4 shows the low temperature ac-susceptibility for $RbAg_2Cr[VO_4]_2$ in emu mole^{-1}, similar to Fig. 4(a). In zero field $\chi_{ac}(T)$ exhibits a broad rounded maximum at $T \approx 1\,\mathrm{K}$ and remains constant below ≈ 300 mK. There are no indications for a magnetic phase transition down to the lowest temperature of our experiment of 0.031 K. Upon increasing the magnetic field to 3 T the maximum shifts to lower temperatures and finally the ac-susceptibility becomes constant below 300 mK. Full polarization, see Figure 4 (b,c), is achieved at temperatures below 300 mK in applied fields of 5.5 T with significantly reduced χ_{ac}-values. An important experimental finding is the observation of hysteric behavior for temperatures below 0.2 K and fields of 0.5 T and 2 T. This is consistent with the opening of a hysteresis in χ_{ac}(B) in field-dependent measurements (Fig. 4 (d)) in a similar field range. We interpret this behavior as the occurrence of a field-induced ordered magnetic phase in this temperature and field range for A = Rb. This interpretation is further supported by the ac-susceptibility data displayed in Figure 4 (d) which shows χ_{ac}(B) at 0.038 K measured with increasing and decreasing magnetic fields. Both curves exhibit a pronounced maximum around 1 T accompanied by hysteretic behavior in the field range $0.5\,\mathrm{T} < B < 2.5\,\mathrm{T}$ which slightly shifts to higher fields and becomes more pronounced with increasing temperature, see also Ref. 33. Such a temperature- and field-dependence of χ(T,B) is not expected for a 1/3 plateau. This anomaly is absent for higher temperatures, e.g. at 2 K. The magnetization data for the series A = Ag, K, and Rb, are given in Figure 4 (c). The individual J-values derived above manifest themselves in different initial slopes of the M(B) curves at 2 K as well as differences in the saturation fields. Magnetic saturation is achieved at $B_s \approx 5\,\mathrm{T}$ and 13.5 T for A = Rb and K, respectively, see also Ref. 33.

C. Specific Heat Data

Finally, we analyze the specific heat data of the three compounds that have been measured in the temperature range between 2 K and 300 K in zero and magnetic fields up to 8 T. Isotypic non-magnetic compounds have been used to account for the lattice contribution to the respective total specific heat. The left panels of Figure 5 show the magnetic part of the specific heat for $AAg_2Cr[VO_4]_2$ with A = Ag, K, and Rb. The distorted TL (A =

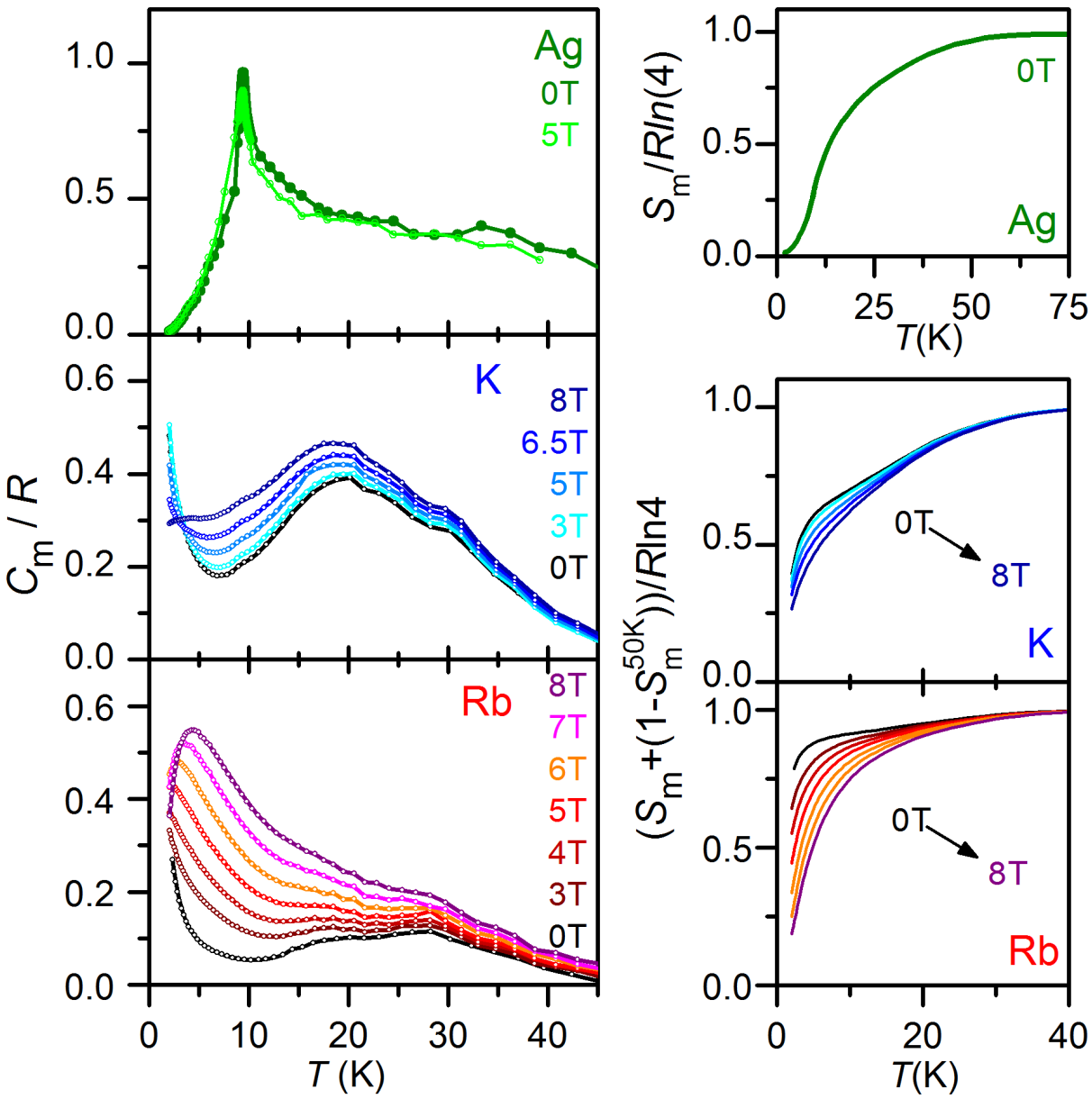

FIG. 5. (*Color online*) *Left*: Field dependence of the magnetic part of the specific heat divided by the gas constant, R, for $AAg_2Cr[VO_4]_2$ with A = Ag (*top*), K (*middle*), Rb (*bottom*). *Right*: Respective magnetic entropy above 2 K. Note that the individual curves are normalized to reach $S_m^{max} = Rln4$ at T = 50 K.

Ag) exhibits a λ-anomaly at $T_N \approx 10$ K, which is not affected by high magnetic fields. We estimate the inter-layer coupling constant ($J_{inter}^{Ag} \approx 0.1$ K) from fitting $C_m \propto T^{336}$ consistent with our DFT calculations, see below.

In contrast to the Ag-compound, the undistorted TL cases (A = K and Rb; space group

$P\bar{3}$) show significantly different behavior in $C_m(T)$ and reveal drastic field dependencies. In particular, the Rb-compound develops a broad maximum in $C_m(T)$ which shifts to higher temperatures with increasing magnetic fields, suggesting the opening of a field-induced gap in the magnetic excitation spectrum. Interestingly, the data suggest the existence of a crossing point of the various $C_m(T, B = \text{const.})$ around 1 K, unfortunately out of the accessible temperature range of our experiment. For the K-compound, however, such a crossing point is revealed around 3 K. According to Ref.[37] such an isobestic point is accompanied by extremal values of $d\chi(T)/dT$ at slightly lower temperatures and discussed as thermodynamic signatures of the crossover from a high-temperature paramagnetic to a low-temperature SL phase. In fact, we observe such extrema in $d\chi(T)/dT$ around 3 K for the A = K compound and around 0.6 K for A = Rb (see Ref. 33) suggestive for the crossover into a low-temperature SL phase.

The derived spin entropy data for the series are shown on the right panel of Figure 4. For the Ag-compound the maximum value of $Rln4 = S_m^{max}$ is reached above $T \approx 50$ K. For the K- and Rb-compounds we shifted the individual curves representing the released spin entropy due to magnetic correlations above 2 K to their values at 50 K. It is noteworthy, that for A = Rb, (K) almost 80% (50 %) of the total spin entropy is retained below $T =$ 2 K in zero field which supports a SL ground state. At high magnetic fields the spin entropy release above 2 K increases significantly for A = Rb and approaches $\approx 75\%$ of S_m^{max} at 8 T. The K-compound behaves similar but overall less sensitive to magnetic fields.

D. *Ab-initio* Calculations

As pointed out above, we find differences in the dominant nearest neighbor (nn) exchange for this series of Cr-compounds. In our experimental work we have demonstrated a significant suppression of LRO from 10 K (A = Ag) to at least 0.031 K (A = K, Rb) by reducing the structural distortion of the TL and the [CrO_6]-complex. The undistorted TL ($P\bar{3}$) allows only for small differences in angles for the local symmetry of the [CrO_6]-complex (D_{3d} and O_h). The calculated single-ion anisotropies for Cr^{3+} in the $AAg_2Cr[VO_4]_2$ series reveal a c-anisotropy for the magnetic moment with $M_{\parallel}^a \approx 0.46$ K and $M_{\parallel}^b \approx 0.88$ K for A = Ag, and $M_{\parallel}^a = M_{\parallel}^b \approx 0.66$ K for A = K and Rb, above the lowest energy state. These estimated values are very small indeed and similar to those reported for $ACrO_2$, which is considered an

easy-axis Heisenberg TL[21]. At any rate, the reduction of the experimental J-couplings from 3 K (Ag) to 0.5 K (Rb) cannot be explained purely on the basis of single-ion anisotropies.

In order to understand these experimental findings we performed electronic structure calculations with density functional theory (DFT) methods and extracted the magnetic exchange constants by mapping total DFT energy differences of various spin configurations onto the Heisenberg Hamiltonian[38–40]. For further results and technical details see Ref. 33, 41, and 42. Analysis of the electronic band structure shows a considerable overlap of V-O states with empty Cr-orbitals ($d_{z^2-r^2}$ and $d_{x^2-y^2}$) for A = K, Rb which effectively reduce the ligand field splitting of the [CrO_6] complex with respect to A = Ag. For calculating the exchange couplings we performed LDA + U calculations and chose values of U that provide J values compatible with the experimental Θ_{CW} values.

The evaluation of the intra-plane exchange couplings confirm an anisotropic TL model for A = Ag with $J_1^{Ag} \approx 2/3\ J_2^{Ag}$ representing the Cr-Cr distances along [010] for the former and the almost equal [110] and [-110] directions for the latter. The small difference for the calculated $J_{2a}^{Ag} = 4.69(1)$ K for [-110] and $J_{2b}^{Ag} = 4.74(1)$ K for [110] is remarkable, as these coupling constants are apparently decisive for the magnetically ordered structure as determined by neutron powder diffraction data, see above. Note that these findings are compatible with a columnar AFM, in line with theoretical work on the anisotropic triangular Heisenberg AFM lattice and the topologically equivalent square lattice with one diagonal bond, see for reference[43].

For the isotropic TL we calculate $J_1^K = 2.8$ K which is similar to J_1^{Ag} and a significantly reduced $J_1^{Rb} = 0.4$ K, respectively. These (nn) values are, in reasonable agreement with the values extracted from the susceptibility measurements. Additionally, DFT calculations allow to disentangle contributions coming from further exchange paths. Overall, intra-plane second (nn) exchange couplings are rather small (≈ 0.01 K) throughout the series and not significant to explain the suppression of LRO to such an extend.

We address now the differences in the inter-planar exchange couplings. These follow two principal stacking types with different relative orientations of the TL along the stacking direction: (i) alternating ABA and (ii) identical AA stacking sequence. First, we comment on the Ag-compound representing the ABA case ($C2/c$). Here, we obtain a weak FM coupling constant, $J_3^{Ag} =$ -0.06 K or 2% in terms of J_1^{Ag}, in nice agreement with our magnetic structure from NPD. In contrast, the inter-layer coupling for the AA stacking ($P\bar{3}$) is different in

two aspects. Firstly, these exchange couplings are AFM. Secondly, the inter-layer coupling constants are about 10% of their respective $J_1^{K,Rb}$ values. Despite the significant amount of the inter-layer exchange couplings, the undistorted TL reveal no signs of LRO as shown in the experiments above.

IV. CONCLUSIONS

In conclusion, we show the drastic reduction of LRO on the AFM TL from 10 K to temperatures at least lower than 0.031 K for a series of $S = 3/2$ compounds, $AAg_2Cr[VO_4]_2$, by altering the size of non-magnetic spacers (A = Ag, K, Rb) between magnetic layers. Our experimental data are consistent with a low-temperature SL phase for the undistorted TL (A = K and Rb). We note an effective reduction of J_1^{Rb} compared with J_1^K, despite the same Cr-Cr distances and only minor variations in Cr-O-Cr angles of less than $\pm 2^\circ$. Structurally, this relates to the differences in the relative orientation of the $[VO_4]$ linkers (coplanar with the TL) while the high-symmetry (three-fold rotation axis) is retained. Electronically, the enhanced hybridization $Cr3d{-}O2p{-}V3d{-}O2p{-}Cr3d$ and the isotropic exchange within the AFM TL are pronounced features of these SL candidates. Further explorations into additional higher order exchange for complex linkers on the undistorted TL are called for and beyond the focus of this experimental work.

V. ACKNOWLEDGMENTS

ACKNOWLEDGMENTS

We gratefully acknowledge funding by the National Science Foundation, (Grant DMR-1149899). The research at ORNL's High Flux Isotope Reactor was sponsored by the Scientific User Facilities Division, Office of Basic Energy Sciences, U.S. Department of Energy. AM also acknowledges funding by the Carl-Zeiss Stiftung. The Frankfurt groups thank the DFG (SFB/TR 49) and PL (DFG-RTG 1952).

---

[1] X.-G. Wen, Phys. Rev. B **65**, 165113 (2002).

[2] L. Balents, Nature **464**, 199 (2010).

[3] F. Mila, Eur. J. Phys. **21**, 499510 (2000).

[4] C. Wang and T. Senthil, Phys. Rev. B **91**, 195109 (2015).

[5] L. Savary and L. Balents, Rep. Prog. Phys. **80**, 016502 (2017), see Tab. 1, Ch. 6.1, and 6.44.

[6] T.-H. Han, J. S. Helton, S. Chu, D. G. Nocera, J. A. Rodriguez-Rivera, C. Broholm, and Y. S. Lee, Nature **492**, 7429 (2012).

[7] B. J. Powell and R. H. McKenzie, Rep. Prog. Phys. **74**, 056501 (2011).

[8] T. Isono, T. Terashima, K. Miyagawa, K. Kanoda, and S. Uji, Nature Comm. **7**, 13494, (2016).

[9] A. P. Ramirez, Annu. Rev. Mater. Sci. **24**, 453-80 (1994).

[10] A. Yu. Kitaev, Ann. Phys. **303**, 2 (2003).

[11] J. Chaloupka, G. Jackeli, and G. Khaliullin, Phys. Rev. Lett. **105**, 027204 (2010).

[12] Y. Shirata, H. Tanaka, A. Matsuo, and K. Kindo, Phys. Rev. Lett. **108**, 057205 (2012).

[13] J. Ma, Y. Kamiya, T. Hong, H.B. Cao, G. Ehlers, W. Tian, C.D. Batista, Z.L. Dun, H.D. Zhou, and M. Matsuda, Phys. Rev. Lett. **116**, 087201 (2016).

[14] B. Bernu, C. L'huillier, and L. Pierre, Phys. Rev. Lett. **69**, 2590 (1992).

[15] H. Kawamura, J. Phys.: Condens. Matter **10**, 4707, (1998).

[16] L. Capriotti, A. E. Trumper, and S. Sorella, Phys. Rev. Lett. **82**, 3899 (1999).

[17] G. H. Wannier, Phys. Rev. **79**, 357 (1950).

[18] S. Seki, Y. Onose, and Y. Tokura, Phys. Rev. Lett. **101**, 067204 (2008).

[19] M. Kenzelmann, G. Lawes, A. B. Harris, G. Gasparovic, C. Broholm, A. P. Ramirez, G. A. Jorge, M. Jaime, S. Park, Q. Huang, A. Ya. Shapiro, and L. A. Demianets, Phys. Rev. Lett. **98**, 267205 (2007).

[20] N. E. Amuneke, J. Tapp, C. R. dela Cruz, and A. Möller, Chem. Mater., **26**, 5930 (2014).

[21] A. Olariu, P. Mendels, F. Bert, B. G. Ueland, P. Schiffer, R. F. Berger, and R. J. Cava, Phys. Rev. Lett. **97**, 167203 (2006).

[22] E. Ghorbani, L. F. Tocchio, and F. Becca, Phys. Rev. B **93**, 085111 (2016).

[23] Y. Iqbal, W.-J. Hu, R. Thomale, D. Poilblanc, and F. Becca, Phys. Rev. B **93**, 144411 (2016).

[24] G. Misguich, C. L'huillier, B. Bernu, and C. Waldtmann, Phys. Rev. B **60**, 1064 (1999).

[25] W. LiMing, G. Misguich, P. Sindzingre, and C. L'huillier, Phys. Rev. B **62**, 6372 (2000).

[26] M. Holt, B. J. Powell, and J. Merino, Phys. Rev. B **89**, 174415 (2014).

[27] M. Roger, J. H. Hetherington, and J. M. Delrieu, Rev. Mod. Physics **55**, 1 (1983).

[28] Magnetic Interactions in Molecules and Solids, C. de Graaf and R. Broer, Springer (Cham, Heidelberg, New York, Dordrecht, London), 2016, see Chap. 5.42.

[29] A. Möller, N.E. Amuneke, P. Daniel, B. Lorenz, C.R. de la Cruz, M. Gooch, P.C.W. Chu, Phys. Rev. B **85**, 214422 (2012).

[30] A. A. Tsirlin, A. Möller, B. Lorenz, Y. Skourski, H. Rosner, Phys. Rev. B **85**, 014401 (2012).

[31] J. Rodríguez-Carvajal, FullProf, version 2.05; Laboratoire Léon Brillouin CEA-CNRS: Gif-sur-Yvette, Cedex, France, 2011.

[32] G. A. Bain, and J. F. Berry, J. Chem. Educ. **85**, 532 (2008).

[33] See Supplemental Material at [URL will be inserted by publisher] for additional experimental and theoretical details, which includes Refs. [37-42].

[34] M. Gerloch and R. F. McMeeking, J. Chem. Soc. Dalton Trans. 2443, (1975).

[35] C. Delmas, G. Le Flem, C. Fouassier, and P. Hagenmuller, J. Phys. Chem. Solids **39**, 55, (1978).

[36] A. Du, G. Z. Wei, and J. Li, Phys. Stat. Sol. B **234**, 636, (2002).

[37] A. P. Ramirez, B. Hessen, and M. Winklemann, Phys. Rev. Lett. **84**, 2957 (2000).

[38] K. Koepernik and H. Eschrig, Phys. Rev. B **59**, 1743 (1999); http://www.FPLO.de

[39] J. P. Perdew, K. Burke and M. Ernzerhof, Phys. Rev. Lett. **77**, 3865 (1996).

[40] A. I. Liechtenstein, V. I. Anisimov, and J. Zaanen, Phys. Rev. B **52**, R5467(R) (1995).

[41] T. Mizokawa, A. Fujimori, Phys. Rev. B **54**, 5368 (1996).

[42] H. O. Jeschke, F. Salvat-Pujol, R. Valentí, Phys. Rev. B **88**, 075106 (2013).

[43] B. Schmidt and P. Thalmeier, Phys. Rev. B **89**, 184402 (2014).